Journal of Computational and Applied Mathematics 401 (2022) 113780

Contents lists available at ScienceDirect

Journal of Computational and Applied Mathematics

journal homepage: www.elsevier.com/locate/cam

# On the cavity detection in a heat conductive medium from time-average boundary temperature measurement

Yuchan Wang [a], Qun Chen [a], Jijun Liu [b,c,*]

[a] School of Mathematics and Statistics, Nanjing University of Information Science and Technology, Nanjing, 210044, PR China
[b] School of Mathematics/S.T. Yau Center of Southeast University, Southeast University, Nanjing, 210096, PR China
[c] Nanjing Center for Applied Mathematics, Nanjing, 211135, PR China

ARTICLE INFO

*Article history:*
Received 16 August 2019
Received in revised form 20 July 2021

*MSC:*
35R30
35K05
47A52
41A60

*Keywords:*
Inverse problem
Shape identification
Regularization
Discrepancy principle
Iteration
Numerics

ABSTRACT

Consider the shape identification of an inclusion in heat conductive medium from the time average measurement, which is modeled by an initial boundary value problem for a parabolic system with extra nonlocal measurement data specified on the outer boundary. For this nonlocal and nonlinear inverse problem for the two-dimensioned parabolic equation in a doubly-connected domain, the radius function describing the shape of inner boundary to be identified is defined as the minimizer of a regularizing cost functional. The existence of this minimizer is firstly proven in a suitable admissible set. Then we establish the convergence rate of the regularizing solution under *a-posteriori* choice strategy for the regularizing parameter. Finally the differentiability of the cost functional is proven, which provides a fundamental basis for gradient type iteration scheme. Based on the adjoint and sensitivity problem of the original problem which give the gradient of the cost functional, we propose a steepest descent iteration algorithm for finding the minimizer approximately. Numerical examples are presented to show the validity of our algorithm.



## 1. Introduction

There are many engineering situations where some ingredients of the conductive system may be unknown, and have to be determined from measurements. These problems are generally called inverse heat conduction problems (IHCP), for example, see [1–4].

A typical problem in IHCP is the boundary shape detection from the measurable temperature on some accessible part of the medium boundary, see [5,6] and the references cited therein. This thermal imaging technique [7], which physically belongs to the category of non-destructive testing of materials, aims at the detections of inclusions or interior cracks of a heat conductor. Besides the technique, in steelworks in modern industries, the outer surface of blast furnace is accessible, to temperature measurements, while the inner surface of the furnace is unaccessible. Therefore, to guarantee the safety of the steel-making process, the important problem is to identify the shape of the inner surface from some extra measurement specified in the outer surface of the blast furnace, see [8].

Let $\Omega_1, \Omega_2 \subset \mathbb{R}^2$ be two simply connected domains satisfying $\overline{\Omega}_1 \subset \Omega_2$ with $C^2$ smooth boundary $\Gamma_i := \partial\Omega_i$ for $i = 1, 2$. Define $\Omega := \Omega_2 \backslash \overline{\Omega}_1$, which represents the 2-dimensional cross section of thermal layer of the furnace, as shown in Fig. 1. In addition, we also assume that both $\Omega_2$ and $\Omega_1$ are starlike, i.e., the boundary can be expressed by

$$\partial\Omega_2 \equiv \Gamma_2 = \{(x_1, x_2) = R(\theta)(\cos\theta, \sin\theta), R(\theta) = R(\theta + 2\pi) > 0, \theta \in [0, 2\pi]\}, \tag{1.1}$$

* Corresponding author at: School of Mathematics/S.T. Yau Center of Southeast University, Southeast University, Nanjing, 210096, PR China.
*E-mail address:* jjliu@seu.edu.cn (J. Liu).

https://doi.org/10.1016/j.cam.2021.113780
0377-0427/

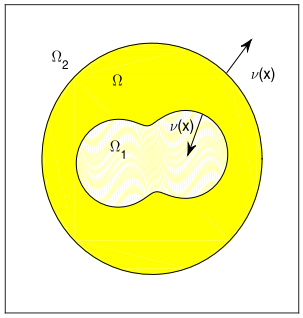


**Fig. 1.** Geometrical configuration of the heat conductive domain $\Omega$ (yellow part). (For interpretation of the references to color in this figure legend, the reader is referred to the web version of this article.)

$$\partial\Omega_1 \equiv \Gamma_1 = \{(x_1, x_2) = r(\theta)(\cos\theta, \sin\theta), R(\theta) > r(\theta) = r(\theta + 2\pi) > 0, \theta \in [0, 2\pi]\}. \tag{1.2}$$

Assume that the temperature $u(x, t)$ in a heat diffusion process is governed by the following parabolic system:

$$\begin{cases} \frac{\partial u}{\partial t} - a^2 \Delta u = 0, & (x, t) \in \Omega \times (0, T) := Q \\ \frac{\partial u}{\partial \nu} = 0, & (x, t) \in \Gamma_1 \times [0, T] \\ \frac{\partial u}{\partial \nu} = \varphi_2(x, t), & (x, t) \in \Gamma_2 \times [0, T] \\ u(x, 0) = 0, & x \in \overline{\Omega}, \end{cases} \tag{1.3}$$

where $\nu(x)$ is the outward unit normal direction to $\partial\Omega$ and $a > 0$ represents the thermal diffusivity. The homogeneous Neumann boundary condition on $\Gamma_1$ means that the inner surface of $\Omega$ is insulated. For known $\Omega$ and $\varphi_2$, the existence and uniqueness of a classical solution and also of a weak solution to the direct problem (1.3) are well-known [9–11].

For detecting the unknown inner boundary $\Gamma_1$, we specify the following time average measurement data of $u$ on the outer boundary

$$\int_0^T \omega(t) u(x, t) dt = f(x), \quad x \in \Gamma_2, \tag{1.4}$$

or its noisy counterpart $f^\delta(x)$ satisfying

$$\left\| f^\delta - f \right\|_{L^2(\Gamma_2)} \le \delta, \tag{1.5}$$

where $0 \le \omega(t) \in L^1(0, T)$ is a given weight function.

The measurement given in the form (1.4) is the so-called time-average data on the boundary, which can weaken the random noise by the average process compared with the point wise measurement $u(x, t)|_{\Gamma_2 \times (0,T)}$ [12]. We notice that the measurement data (1.4) will become local data $u(x, t_1) = f(x)$, if we take the weight function $\omega(t) = \delta(t - t_1)$ [2,13]. So the measurement data (1.4) can be considered as some incomplete data between $u(\cdot, t_1)|_{\Gamma_2}$ and $u(\cdot, \cdot)|_{\Gamma_2 \times (0,T)}$ for recovering $\Gamma_1$. From physical point of view, boundary corrosion arises from a certain accumulated damage [14], consequently the nonlocal measurement (1.4) represents the accumulated effect of using the temperature information in time interval $[0, T]$ and therefore more reasonable, as compared with the local measurement $u(\cdot, t_1)|_{\Gamma_2}$.

By the above motivations, we study the shape identification of a cavity from the nonlocal data (1.4)–(1.5). Due to the possible non-uniqueness of such inversion input for determining $\Gamma_1$, this inverse problem is more ill-posed compared with that using the boundary temperature measurement data

$$u(x, t) = \widetilde{f}(x, t), \quad (x, t) \in \Gamma_2 \times (T_1, T_2) \subset (0, T). \tag{1.6}$$

There already exist many theoretical and numerical results for the shape identification from local measurement in parabolic systems such as (1.6), see [15–22], while the shape identifications using the nonlocal measurement (1.4) are still rather limited. The uniqueness of the inverse boundary value problem with the local measurement data was established in [21], where the Neumann boundary condition is set in the unknown inner boundary, while the Cauchy data in part of the outer boundary is specified. As far as we know, iterative, optimization schemes and sampling-type methods are the main computational tools for numerics. For example, the Newton-type iteration method for the diffusion with Neumann boundary condition and the Landweber method for the diffusion with Dirichlet boundary condition have been applied to identify the boundary shape in [21,22]. Some existing numerical examples in [21] show that the Newton-type iteration method is effective with few iterations when the basis functions for the unknowns are specified appropriately. The Landweber method, which does not need specification of the basis functions, also works well, but it needs more iterations. The other approaches for boundary shape reconstructions are based on optimization schemes for some cost functional. In [18], H. Harbrecht et al. reformulated the shape identification by three different shape optimization problems

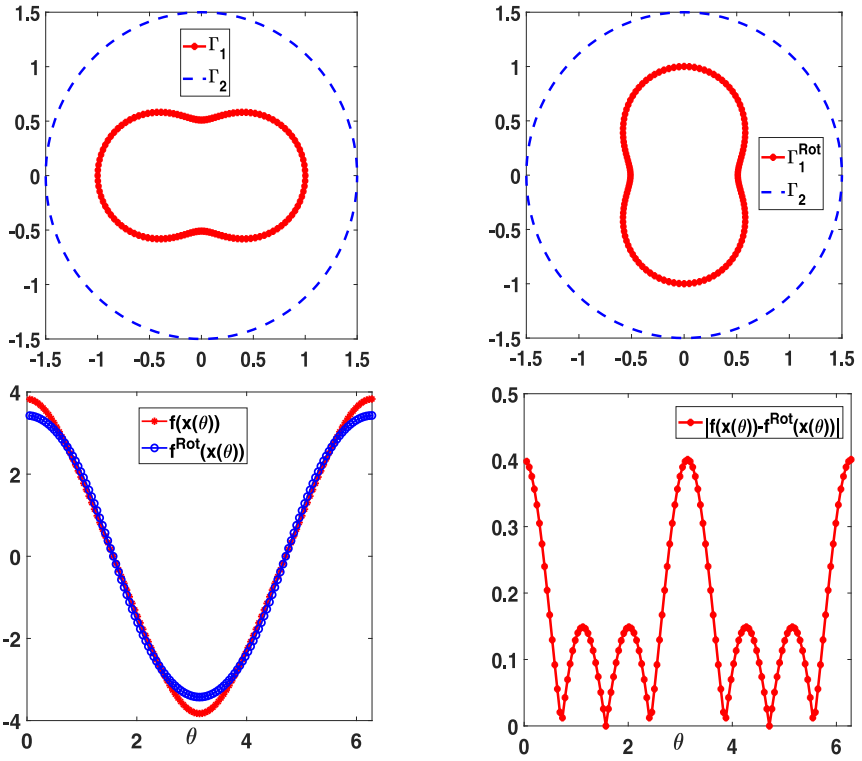


**Fig. 2.** Top line: The doubly-connected domain $\Omega$ with boundary $\Gamma_2 \bigcup \Gamma_1$ (left) and its rotation $\Omega^{Rot}$ (right); Bottom line: $(f(x(\theta)), f^{Rot}(x(\theta)))|_{x(\theta)\in\Gamma_2}$ (left) and the error distribution $\left|f(x(\theta)) - f^{Rot}(x(\theta))\right|_{\theta\in[0,2\pi]}$ (right).

and proposed some iterative methods for exact measurement data. Recently, G. Nakamura and H.B. Wang proposed a sampling-type non-iterative method to reconstruct the boundary and established its rigorous mathematical justification in [16,17]. On the other hand, we would like to emphasize that the detection of $\partial\Omega_1 = \Gamma_1$ can also be realized in case of static thermal fields governed by the Laplace's equation. For this elliptic case, abundant theoretical results and computational tools have been well established, see [23–26] and the references therein.

As stated above, in the case that the inversion input data are given in the form of the Cauchy data in the outer boundary $\Gamma_2$, the recovery of the inner boundary $\Gamma_1$ is unique [21]. Since our nonlocal inversion input data in the integral form (1.4) cannot yield the Dirichlet data $u(\cdot,t)|_{\Gamma_2}$ for given weight function $0 \le \omega \in L^1(0,T)$, there is possibly no uniqueness for our inverse problem. Moreover, there is also possibly no stability result, i.e., input data $f(\cdot)|_{\Gamma_2}$ with small perturbation can correspond to an inner boundary $\Gamma_1$ with large error. To show this fact clearly, consider the concrete form of (1.3)

$$\begin{cases} \frac{\partial u}{\partial t} - \Delta u = 0, & (x,t) = (x_1,x_2,t) \in \Omega \times (0,1) = Q, \\ \frac{\partial u}{\partial \nu} = 0, & (x,t) = (x_1,x_2,t) \in \Gamma_1 \times [0,1], \\ \frac{\partial u}{\partial \nu} = \varphi_2(x,t) := x_1 \exp(-4t+2), & (x,t) = (x_1,x_2,t) \in \Gamma_2 \times [0,1], \\ u(x,0) = 0, & x = (x_1,x_2) \in \overline{\Omega} \end{cases} \tag{1.7}$$

with the boundary $\partial\Omega = \Gamma_1 \bigcup \Gamma_2$ of thedomain $\Omega$ defined by

$$\partial\Omega_2 \equiv \Gamma_2 = \{x : (x_1,x_2) = 1.5(\cos\theta, \sin\theta),\ \theta \in [0,2\pi]\},$$
$$\partial\Omega_1 \equiv \Gamma_1 = \{x : (x_1,x_2) = \sqrt{\cos^2\theta + 0.26\sin^2\theta}(\cos\theta, \sin\theta),\ \theta \in [0,2\pi]\},$$

see top (left) in Fig. 2.

Now we rotate the domain $\Omega$ by $\frac{\pi}{2}$ clockwise to yield the domain

$$\Omega^{Rot} := (\Omega_2 \setminus \overline{\Omega}_1)^{Rot} = \Omega_2 \setminus \overline{\Omega}_1^{Rot}$$
$$= \left\{ x = (x_1,x_2) : \begin{pmatrix} x_1 \\ x_2 \end{pmatrix} = \begin{pmatrix} 0 & 1 \\ -1 & 0 \end{pmatrix} \begin{pmatrix} z_1 \\ z_2 \end{pmatrix},\ \forall\, (z_1,z_2) \in \Omega \right\},$$

see top (right) in Fig. 2. Denote by $u^{Rot}(x,t)$ the solution to (1.7) with $\Omega$ replaced by $\Omega^{Rot}$ and the same Neumann data $\varphi_2(x,t)$ in $\Gamma_2$. We can firstly compute $(u(x,t), u^{Rot}(x,t))$ for $(x,t) \in \Gamma_2 \times [0,1]$ numerically using the boundary integral

equation method (BIEM) [21], and then generate the nonlocal inversion input data $f|_{\Gamma_2}, f^{Rot}|_{\Gamma_2}$ corresponding to $u, u^{Rot}$ from (1.4) with specified $\omega(t) \equiv 1,\ t \in [0, T] = [0, 1]$. The functions $f|_{\Gamma_2}, f^{Rot}|_{\Gamma_2}$ as well as their difference are shown in the bottom line of Fig. 2. It can be seen clearly that, although we have $f|_{\Gamma_2} \approx f^{Rot}|_{\Gamma_2}$, the interior boundaries $\Gamma_1$ and $\Gamma_1^{Rot}$ are completely different.

The novel contributions of this work contain the following three points. Firstly, we consider the thermal imaging technique for detecting the boundary $\partial\Omega_1$ of the inner cavity $\Omega_1$ from the nonlocal input data (1.4). Such kind of data can represent the accumulated damage of a corrosion process. Secondly, we give a rigorous analysis of the optimization version of this inverse problem, including the existence of the minimizer and a choice strategy for the regularizing parameter. Finally, we also establish the error estimates on both the datafit and the solution approximation. Numerical implementations verify our theoretical results well.

This paper is organized as follows. Firstly, we reformulate the inverse problem as an optimization problem for some Tikhonov functional in Section 2. The existence of the minimizer of the cost functional is proven in some admissible set, which ensures the reasonability of the generalized solution. The error estimate on the regularizing solution using the *a-posterior* choice strategy for the regularizing parameter is established under some source condition for the exact solution. Then we prove the differentiability of the cost functional and compute its Fréchet derivative rigorously in Section 3, which provides the fundamentals for the steepest descent iterations for our reconstruction algorithm. The optimal iteration times are also analyzed, which is crucial to weakening the computational cost. The numerical examples are presented in Section 4, showing the validity of our proposed scheme. Finally we give some conclusions in Section 5.

## 2. Reformulation of the inverse problem

Assume that the origin $\mathbf{0} \in \Omega_1 \subset \Omega_2$. We firstly reformulate the inverse problem as an optimizing problem. Introduce the admissible set

$$\mathcal{A} := \{r(\theta) \in C^2(0, 2\pi) : r(\theta) = r(\theta + 2\pi),\ 0 \le r(\theta) < R(\theta),\ \|r'\|_{L^2(0,2\pi)} \le M_0\}$$

for $r(\theta)$ representing the radius of the interior boundary $\Gamma_1$ to be identified, where $R(\theta)$ is the radius of the known outer boundary $\Gamma_2$. Obviously, $\|r\|_{H^1(0,2\pi)}$ is uniformly bounded for $r \in \mathcal{A}$.

Now we establish the Tikhonov type regularizing scheme for our inverse problem. For the direct problem (1.3) with the inner boundary $\Gamma_1$ representing by $r(\theta)$, denoted by $u[r](x, t)$ its solution. For the noisy data $f^\delta$ satisfying (1.5), we consider the cost functional

$$J_\alpha^\delta(r) := \left\| \int_0^T \omega(t) u[r](\cdot, t) dt - f^\delta(\cdot) \right\|^2_{L^2(\Gamma_2)} + \alpha \|r\|^2_{L^2(0,2\pi)} \tag{2.1}$$

with regularizing parameter $\alpha > 0$. Then we will find the minimizer $r^{\alpha,\delta}$ of $J_\alpha^\delta(r)$ in $\mathcal{A}$ for specified small parameter $\alpha$, which will be regarded as the regularizing solution to our shape identification problem. Since the solution to our inverse problem with the exact inversion data $f(x)$ may not be unique as explained in Section 1, we define the minimum norm solution $r^+$ for exact input data by

$$\|r^+\|_{L^2(0,2\pi)} := \min_{r \in \mathcal{A}} \left\{ \|r\|_{L^2(0,2\pi)} :\ \int_0^T \omega(t) u[r](x, t) dt = f(x) \text{ for } x \in \Gamma_2 \right\}. \tag{2.2}$$

Due to the compactness of $\mathcal{A}$ in $L^2(0, 2\pi)$, the existence of $r^+(\theta)$ defined in terms of (2.2) is obvious. However, $r^+$ may not be unique. In the sense that $r^+$ yields the boundary data which match up the exact inversion data $f(x)$ from the exact boundary $\Gamma_1$, we consider

$$\Gamma_1^+ := \{x := r^+(\theta)(\cos\theta, \sin\theta) :\ \theta \in [0, 2\pi]\}$$

as the exact inner boundary. We will estimate the error between regularizing solution $r^{\alpha,\delta}$ and $r^+$ in the sequel for *a-posteriori* choice strategy for $\alpha > 0$. More precisely, we apply the Morozov's discrepancy principle (MDP) to determine $\alpha$, i.e., $\alpha$ is chosen such that the corresponding minimizer $r^{\alpha,\delta}$ of (2.1) meets

$$\left\| \int_0^T \omega(t) u[r^{\alpha,\delta}](\cdot, t) dt - f^\delta(\cdot) \right\|_{L^2(\Gamma_2)} = \mu\delta \tag{2.3}$$

with some specified $\mu > 1$, which is chosen artificially.

The following existence result for the minimizer $r^{\alpha,\delta}$ ensures the reasonability of our generalized solution for specified $\alpha > 0$.

**Theorem 2.1.** *For known outer boundary $\Gamma_2$, the optimization version*

$$\inf\{J_\alpha^\delta(r) : r \in \mathcal{A}\} \tag{2.4}$$

*of the original inverse boundary problem (1.3)–(1.5) has a solution $r^{\alpha,\delta} \in \mathcal{A}$ for fixed $\alpha, \delta > 0$.*

**Proof.** Obviously, $J_\alpha^\delta(r) \geq 0$ for all $r \in \mathcal{A}$. Then we can define

$$\inf\{J_\alpha^\delta(r) : r \in \mathcal{A}\} := M_1(\omega, \alpha, f^\delta, M_0) \equiv M_1 \geq 0.$$

Let $\{r^n : n \in \mathbb{N}\} \subset \mathcal{A}$ be the minimizing sequence, i.e., $\lim_{n\to\infty} J_\alpha^\delta(r^n) = M_1$, which says

$$\|r^n\|^2_{L^2(0,2\pi)} \leq \frac{J_\alpha^\delta(r^n)}{\alpha} \leq \frac{C(M_1)}{\alpha} \text{ for all } n = 0, 1, \ldots.$$

On the other hand, $r^n \in \mathcal{A}$ means that $\|(r^n)'\|_{L^2(0,2\pi)} \leq M_0$. By Arzela theorem, there exists a subsequence of $\{r^n : n \in \mathbb{N}\}$ converging to some $r_* \in L^2(0, 2\pi)$ with $0 \leq r_*(\theta) \leq R(\theta)$ in $L^2(0, 2\pi)$. For simplicity of the notations, we still denote by $\{r^n : n \in \mathbb{N}\}$ this subsequence.

By Theorem 2.1 in [21], the cost functional $J_\alpha^\delta(r)$ is weak lower semi-continuous with respect to $r$, i.e., it follows that

$$J_\alpha^\delta(r_*) \leq \lim_{n\to\infty} J_\alpha^\delta(r^n) = M_1,$$

so $r_*$ is the minimizer of $J_\alpha^\delta(r)$ in $\mathcal{A}$, which is taken as $r^{\alpha,\delta}$, the approximate solution of the inverse problem (1.3)–(1.5) for the noisy input data $f^\delta(x)$. The proof is complete. □

The important issue for our regularizing solution is that the choice strategy for $\alpha$ in terms of (2.3) is implementable. By the analogous arguments used in [27,28], we have the following result.

**Theorem 2.2.** *For fixed $(\varphi_2, f^\delta)$ and $\mu > 1$, assume that the solution $\widehat{u}(x, t)$ to the direct problem (1.3) with $\Omega = \Omega_2$ (i.e., $\Omega_1 = \emptyset$) satisfies*

$$\left\| \int_0^T \omega(t)\widehat{u}(\cdot, t)dt - f(\cdot) \right\|_{L^2(\Gamma_2)} > (\mu + 1)\delta. \tag{2.5}$$

*Then there exists a parameter $\alpha := \alpha^* \in \left[ \frac{(\mu^2-1)\delta^2}{\|r^+\|^2_{L^2(0,2\pi)}}, \infty \right)$ to (2.3) for fixed $r^+$ solving (2.2).*

**Proof.** Denote by $r^{\alpha_i,\delta}$ the minimizer of cost functional (2.1) in $\mathcal{A}$ corresponding to $\alpha = \alpha_i$ with $i = 1, 2$. Then we have

$$\begin{aligned} &\left\| \int_0^T \omega(t)u[r^{\alpha_1,\delta}](\cdot, t)dt - f^\delta(\cdot) \right\|^2_{L^2(\Gamma_2)} + \alpha_1 \|r^{\alpha_1,\delta}\|^2_{L^2(0,2\pi)} \\ \leq &\left\| \int_0^T \omega(t)u[r^{\alpha_2,\delta}](\cdot, t)dt - f^\delta(\cdot) \right\|^2_{L^2(\Gamma_2)} + \alpha_1 \|r^{\alpha_2,\delta}\|^2_{L^2(0,2\pi)}, \end{aligned}$$

and

$$\begin{aligned} &\left\| \int_0^T \omega(t)u[r^{\alpha_2,\delta}](\cdot, t)dt - f^\delta(\cdot) \right\|^2_{L^2(\Gamma_2)} + \alpha_2 \|r^{\alpha_2,\delta}\|^2_{L^2(0,2\pi)} \\ \leq &\left\| \int_0^T \omega(t)u[r^{\alpha_1,\delta}](\cdot, t)dt - f^\delta(\cdot) \right\|^2_{L^2(\Gamma_2)} + \alpha_2 \|r^{\alpha_1,\delta}\|^2_{L^2(0,2\pi)}. \end{aligned}$$

The above two inequalities yield

$$(\alpha_1 - \alpha_2)\left( \left\| \int_0^T \omega(t)u[r^{\alpha_1,\delta}](\cdot, t)dt - f^\delta(\cdot) \right\|^2 - \left\| \int_0^T \omega(t)u[r^{\alpha_2,\delta}](\cdot, t)dt - f^\delta(\cdot) \right\|^2 \right) \geq 0,$$

which implies that $\left\| \int_0^T \omega(t)u[r^{\alpha,\delta}](\cdot, t)dt - f^\delta(\cdot) \right\|^2_{L^2(\Gamma_2)}$ is an increasing function with respect to $\alpha$.

On the other hand, we also have

$$\begin{aligned} 0 &\le \lim_{\alpha\to\infty} \left\|r^{\alpha,\delta}\right\|^2_{L^2(0,2\pi)} \le \lim_{\alpha\to\infty} \frac{J_\alpha(r^{\alpha,\delta})}{\alpha} \le \lim_{\alpha\to\infty} \frac{J_\alpha(0)}{\alpha} \\ &\le \lim_{\alpha\to\infty} \frac{\left\|\int_0^T \omega(t)\widehat{u}(\cdot,t)dt - f^\delta(\cdot)\right\|^2_{L^2(\Gamma_2)}}{\alpha} \\ &\le \lim_{\alpha\to\infty} \frac{2\left\|\omega\right\|^2_{L^2(0,T)}\left\|\hat{u}\right\|^2_{L^2(\Gamma_2\times(0,T))} + 2\left\|f^\delta\right\|^2_{L^2(\Gamma_2)}}{\alpha} = 0. \end{aligned}$$

Due to this estimate and also $r^{\alpha,\delta}(\theta) \ge 0$, we have $\lim_{\alpha\to\infty} r^{\alpha,\delta}(\theta) = 0$ for $\theta \in [0, 2\pi]$, i.e., $\lim_{\alpha\to\infty} \Omega_1^{\alpha,\delta} = \emptyset$, or, equivalently,

$$\lim_{\alpha\to\infty} \Omega_2 \backslash \overline{\Omega_1^{\alpha,\delta}} = \Omega_2.$$

Therefore, we have

$$\begin{aligned} &\lim_{\alpha\to\infty} \left\|\int_0^T \omega(t)u[r^{\alpha,\delta}](\cdot,t)dt - f^\delta(\cdot)\right\|_{L^2(\Gamma_2)} \\ &= \lim_{\alpha\to\infty} \left\|\int_0^T \omega(t)u[r^{\alpha,\delta}](\cdot,t)dt - f(\cdot) + f(\cdot) - f^\delta(\cdot)\right\|_{L^2(\Gamma_2)} \\ &\ge \lim_{\alpha\to\infty} \left\|\int_0^T \omega(t)u[r^{\alpha,\delta}](\cdot,t)dt - f(\cdot)\right\|_{L^2(\Gamma_2)} - \left\|f - f^\delta\right\|_{L^2(\Gamma_2)} \\ &\ge \left\|\int_0^T \omega(t)\widehat{u}(\cdot,t)dt - f(\cdot)\right\|_{L^2(\Gamma_2)} - \delta > \mu\delta \end{aligned} \tag{2.6}$$

in terms of (2.5). Moreover, for $\alpha_0 = \frac{(\mu^2-1)\delta^2}{\|r^+\|^2_{L^2(0,2\pi)}}$, we also have that

$$\begin{aligned} &\left\|\int_0^T \omega(t)u[r^{\alpha_0,\delta}](\cdot,t)dt - f^\delta(\cdot)\right\|^2_{L^2(\Gamma_2)} \le J_{\alpha_0}(r^{\alpha_0,\delta}) \\ &\le \left\|\int_0^T \omega(t)u[r^+](\cdot,t)dt - f^\delta(\cdot)\right\|^2_{L^2(\Gamma_2)} + \alpha_0\|r^+\|^2_{L^2(0,2\pi)} \le \mu^2\delta^2. \end{aligned} \tag{2.7}$$

Since $\left\|\int_0^T \omega(t)u[r^{\alpha,\delta}](\cdot,t)dt - f^\delta(\cdot)\right\|^2_{L^2(\Gamma_2)}$ is an increasing continuous function with respect to $\alpha > 0$, (2.6)–(2.7) imply that there exists a solution $\alpha^* \in \left[\frac{(\mu^2-1)\delta^2}{\|r^+\|^2_{L^2(0,2\pi)}}, \infty\right)$ to (2.3). The proof is complete. □

**Remark 2.3.** For any fixed $\mu > 1$, since the exact input data $f(x)$ are from $\Omega$ with some inclusion $\Omega_1$, the condition (2.5) always holds for nonempty cavity $\Omega_1$ and small $\delta > 0$.

To establish the convergence rate of regularizing solution, we introduce the following source condition for the exact solution $r^+$ defined in (2.2). The analogous source condition was also assumed in [27,28] for obtaining convergence rate in terms of the Morozov's discrepancy principle.

$\mathcal{SC}2.1$ : For $r^+$ defined in (2.2), there exist two constants $c_1, \tau \in (0, 1)$ such that

$$2|\langle r^+, r - r^+\rangle| \le c_1\|r - r^+\|^2_{L^2(0,2\pi)} + \left\|\int_0^T \omega(t)(u[r](\cdot,t) - u[r^+](\cdot,t))dt\right\|^{2\tau}_{L^2(\Gamma_2)} \tag{2.8}$$

holds for all $r \in \mathcal{A}$, where $\langle\cdot,\cdot\rangle$ is the inner product in $L^2(0, 2\pi)$.

As explained before, $r^+$ defined in terms of (2.2) may not be unique. However, under the extra assumption that the minimum norm solution meets (2.8), we have

**Lemma 2.4.** *If the minimum norm solution $r^+$ also meets (2.8), then it is unique.*

**Proof.** Assume we have two minimum norm solutions $r_1^+$ and $r_2^+$ in $\mathcal{A}$. Then for $r_1^+$ meeting (2.8), we have by taking $r = r_2^+ \in \mathcal{A}$ that

$$\begin{aligned} 2|\langle r_1^+, r_2^+ - r_1^+\rangle| &\le c_1\|r_2^+ - r_1^+\|^2_{L^2(0,2\pi)} + \left\| \int_0^T \omega(t)(u[r_2^+](\cdot,t) - u[r_1^+](\cdot,t))dt \right\|^{2\tau}_{L^2(\Gamma_2)} \\ &= c_1\|r_2^+ - r_1^+\|^2_{L^2(0,2\pi)}, \end{aligned}$$

since $r_1^+, r_2^+ \in \mathcal{A}$. On the other hand, we have

$$\|r_2^+ - r_1^+\|^2_{L^2(0,2\pi)} \equiv \|r_2^+\|^2_{L^2(0,2\pi)} - \|r_1^+\|^2_{L^2(0,2\pi)} - 2\langle r_1^+, r_2^+ - r_1^+\rangle \le -2\langle r_1^+, r_2^+ - r_1^+\rangle,$$

noticing that $r_2^+$ is also the minimum norm solution. The above two estimates yield

$$\|r_2^+ - r_1^+\|^2_{L^2(0,2\pi)} \le c_1\|r_2^+ - r_1^+\|^2_{L^2(0,2\pi)}$$

for $0 < c_1 < 1$, i.e., $\|r_2^+ - r_1^+\|^2_{L^2(0,2\pi)} = 0$. The proof is complete. □

Since $r^+$ is unique under the source condition $\mathcal{SC}2.1$, we can analyze the error between $r^+$ and our regularizing solution.

**Theorem 2.5.** *Let the source condition $\mathcal{SC}2.1$ hold for $r^+$. For the regularization parameter $\alpha$ chosen according (2.3), we have the error estimates*

$$\begin{aligned} \left\| \int_0^T \omega(t)u[r^{\alpha,\delta}](\cdot,t)dt - \int_0^T \omega(t)u[r^+](\cdot,t)dt \right\|_{L^2(\Gamma_2)} &\le (\mu+1)\delta, \\ \|r^{\alpha,\delta} - r^+\|_{L^2(0,2\pi)} &\le \frac{1}{\sqrt{1-c_1}}(\mu+1)^\tau\delta^\tau, \end{aligned}$$

*where $r^{\alpha,\delta}$ is the minimizer of (2.1) for $\mu > 1, 0 < \tau < 1$.*

**Proof.** Since $r^{\alpha,\delta}$ is the minimizer, we have

$$\begin{aligned} &\left\| \int_0^T \omega(t)u[r^{\alpha,\delta}](\cdot,t)dt - f^\delta(\cdot) \right\|^2_{L^2(\Gamma_2)} + \alpha\|r^{\alpha,\delta}\|^2_{L^2(0,2\pi)} \\ \le &\left\| \int_0^T \omega(t)u[r^+](\cdot,t)dt - f^\delta(\cdot) \right\|^2_{L^2(\Gamma_2)} + \alpha\|r^+\|^2_{L^2(0,2\pi)} \le \delta^2 + \alpha\|r^+\|^2_{L^2(0,2\pi)}, \end{aligned}$$

which yields for $\mu > 1$ and $\alpha$ chosen by (2.3) that

$$\|r^{\alpha,\delta}\|^2_{L^2(0,2\pi)} - \|r^+\|^2_{L^2(0,2\pi)} = \frac{(1-\mu^2)\delta^2}{\alpha} < 0. \tag{2.9}$$

On the other hand, we have that

$$\begin{aligned} &\left\| \int_0^T \omega(t)(u[r^{\alpha,\delta}](\cdot,t) - u[r^+](\cdot,t))dt \right\|_{L^2(\Gamma_2)} \\ \le &\left\| \int_0^T \omega(t)u[r^{\alpha,\delta}](\cdot,t)dt - f^\delta(\cdot) \right\|_{L^2(\Gamma_2)} + \left\| f^\delta(\cdot) - \int_0^T \omega(t)u[r^+](\cdot,t)dt \right\|_{L^2(\Gamma_2)} \\ = &\ \mu\delta + \left\| f^\delta(\cdot) - f(\cdot) \right\|_{L^2(\Gamma_2)} \le (\mu+1)\delta. \end{aligned} \tag{2.10}$$

Under the source condition $\mathcal{SC}2.1$, by inequality (2.9), it follows that

$$\begin{aligned} &\|r^{\alpha,\delta} - r^+\|^2_{L^2(0,2\pi)} \\ = &\|r^{\alpha,\delta}\|^2_{L^2(0,2\pi)} - \|r^+\|^2_{L^2(0,2\pi)} - 2\langle r^+, r^{\alpha,\delta} - r^+\rangle \\ \le &\ c_1\|r^{\alpha,\delta} - r^+\|^2_{L^2(0,2\pi)} + \left\| \int_0^T \omega(t)(u[r^{\alpha,\delta}](\cdot,t) - u[r^+](\cdot,t))dt \right\|^{2\tau}_{L^2(\Gamma_2)}, \end{aligned}$$

which generates

$$\begin{aligned} \|r^{\alpha,\delta} - r^+\|_{L^2(0,2\pi)} &\le \frac{1}{\sqrt{1-c_1}} \left\| \int_0^T \omega(t)(u[r^{\alpha,\delta}](\cdot,t) - u[r^+](\cdot,t))dt \right\|^\tau_{L^2(\Gamma_2)} \\ &\le \frac{1}{\sqrt{1-c_1}}(\mu+1)^\tau\delta^\tau \end{aligned}$$

by (2.10). The proof is complete. □

**Remark 2.6.** It is well-known that, for nonlinear inverse problems, some source conditions on the unknown are necessary for establishing the convergence rate in general. Since $r^+$ is the exact boundary and $\mathcal{A}$ is our admissible set for reconstruction, $r - r^+$ is the error between the exact solution $r^+$ and the possible solution $r \in \mathcal{A}$. The left hand side of (2.8) is essentially the first order error, while the first term on the right hand side is the second order error. For our condition $\mathcal{SC}2.1$, it can be explained as the requirement that the error $r - r^+$ on the left hand side should be bounded by the quadratic term $\|r - r^+\|^2$ together with the corresponding data match error in $\Gamma_2$ (the second term of the right hand side in (2.8)) as extra compensation, which is essentially determined by the unknown cavity $\Omega_1$ represented by $r^+$. Notice, it is impossible in general to bound the first order small quantity by its quadratic form. Without such a source condition, we can still get the data-fit error $(\mu + 1)\delta$ yielding from the regularizing solution $r^{\alpha,\delta}$ and $r^+$, but no norm error between $r^{\alpha,\delta}$ and $r^+$ can be established.

## 3. Numerical implementations

Obviously, the optimization version $\inf\{J_\alpha^\delta(r) : r \in \mathcal{A}\}$ for our inverse problem is a constraint optimization problem about the data-fit term of input data for the elements $r$ with uniform bounds on $\|r\|_2$, $\|r'\|_2$. So we consider the following unconstraint optimization problem

$$\begin{aligned} r^{\alpha,\delta} &:= \inf_{r\in\mathcal{A}} \bar{J}_\alpha^\delta(r); \\ \bar{J}_\alpha^\delta(r) &:= \left\| \int_0^T \omega(t) u[r](\cdot, t)dt - f^\delta(\cdot) \right\|^2_{L^2(\Gamma_2)} + \alpha \|r\|^2_{H^1(0,2\pi)} \end{aligned} \tag{3.1}$$

directly in the following numerical implementations.

Next we will deduce the Fréchet derivative of cost functional $\bar{J}_\alpha^\delta(r)$ with respect to $r$. For inner boundary $\Gamma_1$ with radius $r(\theta) \in \mathcal{A}$, consider its perturbation direction

$$d(\theta) := q(\theta)(\cos\theta, \sin\theta),$$

where $q(\theta) \in C^2(0, 2\pi)$ satisfying $q(\theta) = q(\theta + 2\pi)$ for $\theta \in [0, 2\pi]$.

For $\epsilon > 0$ small enough, denote by $r_\epsilon := r + \epsilon q \in \mathcal{A}$, which is the representation of inner boundary

$$\Gamma_1^\epsilon := \{(x_1, x_2) = (r(\theta) + \epsilon q(\theta))(\cos\theta, \sin\theta) : \theta \in [0, 2\pi]\}$$

of cavity $\Omega_1^\epsilon \subseteq \Omega_2$. Now we introduce the domain derivative

$$u'[r; q](x, t)|_{\Gamma_2\times(0,T)} := \lim_{\epsilon\to 0} \frac{u[r_\epsilon](x, t)|_{\Gamma_2\times(0,T)} - u[r](x, t)|_{\Gamma_2\times(0,T)}}{\epsilon}$$

to deduce the Fréchet derivative of $\bar{J}_\alpha^\delta(r)$ along direction $d$. By straightforward computations, $u'(x, t)$ satisfies the following sensitivity problem

$$\begin{cases} \frac{\partial u'}{\partial t} - a^2 \Delta u' = 0, & (x, t) \in Q \\ \frac{\partial u'}{\partial \nu} = -\left(\frac{rq}{\sqrt{r^2+r'^2}}\right) \frac{\partial u}{\partial t} + \frac{\partial}{\partial s}\left(\left(\frac{rq}{\sqrt{r^2+r'^2}}\right) \frac{\partial u}{\partial s}\right), & (x, t) \in \Gamma_1 \times [0, T] \\ \frac{\partial u'}{\partial \nu} = 0, & (x, t) \in \Gamma_2 \times [0, T] \\ u'(x, 0) = 0, & x \in \overline{\Omega}, \end{cases} \tag{3.2}$$

where $\frac{\partial}{\partial s}$ denotes the derivative with respect to arc length on $\Gamma_1$, and $u(x, t) = u[r](x, t)$ is the solution to the direct problem.

The next result shows the differentiability of $\bar{J}_\alpha^\delta(r)$ with respect to $r$, which forms the theoretical fundamental on the gradient-type iteration algorithm for minimizing the cost functional.

**Theorem 3.1.** *The functional $\bar{J}_\alpha^\delta(r)$ is Fréchet differentiable with respect to $r \in \mathcal{A}$. The derivative at $\Gamma_1$ along direction $d$ has the representation*

$$\begin{aligned} \nabla \bar{J}_\alpha^\delta(r) \circ q = 2 \int_0^{2\pi} q(\theta) r(\theta) \left( \int_0^T v(x(\theta), t) \frac{\partial u(x(\theta), t)}{\partial t} + \frac{\partial u(x(\theta), t)}{\partial s} \frac{\partial v(x(\theta), t)}{\partial s} \right) dt\, d\theta + \\ 2\alpha \int_0^{2\pi} q(\theta)(r(\theta) - r''(\theta)) d\theta, \end{aligned} \tag{3.3}$$

*where $x(\theta) = r(\theta)(\cos\theta, \sin\theta)$, and $v(x, t)$ is the solution to the adjoint system*

$$\begin{cases} -\frac{\partial v}{\partial t} - a^2 \Delta v = 0, & (x, t) \in Q \\ \frac{\partial v}{\partial \nu} = 0, & (x, t) \in \Gamma_1 \times [0, T] \\ \frac{\partial v}{\partial \nu} = -\omega(t) \left( \int_0^T \omega(t) u[r](x, t)dt - f^\delta(x) \right), & (x, t) \in \Gamma_2 \times [0, T] \\ v(x, T) = 0, & x \in \overline{\Omega}. \end{cases} \tag{3.4}$$

**Proof.** Let $u[r_\epsilon](x,t)$ be the solution of forward problem (1.3) with inner boundary $\Gamma_1^\epsilon$. Based on the sensitivity problem (3.2), we have

$$\begin{aligned} & u[r_\epsilon](x,t)|_{(x,t)\in\Gamma_2\times(0,T)} \\ =\ & u[r](x,t)|_{(x,t)\in\Gamma_2\times(0,T)}+\epsilon u'[r;q](x,t)|_{(x,t)\in\Gamma_2\times(0,T)}+O(\epsilon^2). \end{aligned} \tag{3.5}$$

Since

$$\begin{aligned} & \bar{J}_\alpha^\delta(r_\epsilon)-\bar{J}_\alpha^\delta(r) \\ =\ & \left\|\int_0^T \omega(t)u[r_\epsilon](\cdot,t)dt-f^\delta(\cdot)\right\|^2_{L^2(\Gamma_2)}-\left\|\int_0^T \omega(t)u[r](\cdot,t)dt-f^\delta(\cdot)\right\|^2_{L^2(\Gamma_2)}+ \\ & \alpha\left(\|r+\epsilon q\|^2_{H^1(0,2\pi)}-\|r\|^2_{H^1(0,2\pi)}\right) \\ =\ & \int_{\Gamma_2}\left(\int_0^T \omega(t)(u[r_\epsilon]+u[r])(x,t)dt-2f^\delta(x)\right)\left(\int_0^T \omega(t)(u[r_\epsilon]-u[r])(x,t)dt\right)ds(x)+ \\ & \alpha\epsilon\left(\int_0^{2\pi} q(\theta)(2r(\theta)+\epsilon q(\theta))d\theta+\int_0^{2\pi} q'(\theta)(2r'(\theta)+\epsilon q'(\theta))d\theta\right), \end{aligned}$$

we can derive

$$\begin{aligned} & \lim_{\epsilon\to 0}\frac{\bar{J}_\alpha^\delta(r_\epsilon)-\bar{J}_\alpha^\delta(r)}{\epsilon} \\ =\ & 2\int_{\Gamma_2}\left(\int_0^T \omega(t)u[r](x,t)dt-f^\delta(x)\right)\left(\int_0^T \omega(t)u'[r;q](x,t)dt\right)ds(x)+ \\ & 2\alpha\left(\int_0^{2\pi} q(\theta)r(\theta)d\theta+\int_0^{2\pi} q'(\theta)r'(\theta)d\theta\right) \\ =\ & 2\int_{\Gamma_2}\int_0^T \omega(t)\left(\int_0^T \omega(t)u[r](x,t)dt-f^\delta(x)\right)u'[r;q](x,t)dtds(x)+ \\ & 2\alpha\int_0^{2\pi} q(\theta)(r(\theta)-r''(\theta))d\theta \end{aligned} \tag{3.6}$$

from (3.5) and $r''(0)=r''(2\pi)$, $q(0)=q(2\pi)$. By subtracting two boundary value problems (3.2) and (3.4) and applying the divergence theorem, we have

$$\begin{aligned} 0 =\ & \int_\Omega\int_0^T v(u'_t-a^2\triangle u')dtdx \\ =\ & \left(\int_\Omega u'vdx\right)\Big|_0^T-\int_\Omega\int_0^T v_t u'dtdx- \\ & a^2\left(\int_0^T\int_{\partial\Omega} v\frac{\partial u'}{\partial\nu}-u'\frac{\partial v}{\partial\nu}ds(x)dt+\int_0^T\int_\Omega u'\triangle v dxdt\right) \\ =\ & \int_0^T\int_\Omega u'(-v_t-a^2\triangle v)dxdt-a^2\int_0^T\int_{\partial\Omega}\left(v\frac{\partial u'}{\partial\nu}-u'\frac{\partial v}{\partial\nu}\right)ds(x)dt \\ =\ & -a^2\int_0^T\int_{\partial\Omega}\left(v\frac{\partial u'}{\partial\nu}-u'\frac{\partial v}{\partial\nu}\right)ds(x)dt \\ =\ & -a^2\left(\int_0^T\int_{\Gamma_1} v\frac{\partial u'}{\partial\nu}ds(x)dt-\int_0^T\int_{\Gamma_2} u'\frac{\partial v}{\partial\nu}ds(x)dt\right). \end{aligned}$$

Moreover, since both $r(\theta)$ and $q(\theta)$ are $2\pi$-periodic functions, we have

$$\begin{aligned} & \int_{\Gamma_2}\int_0^T \omega(t)\left(\int_0^T \omega(t)u[r](x,t)dt-f^\delta(x)\right)u'[r;q](x,t)dtds(x) \\ =\ & \int_{\Gamma_2}\int_0^T -\frac{\partial v(x,t)}{\partial\nu}u'[r;q](x,t)dtds(x) \\ =\ & \int_{\Gamma_1}\int_0^T -\frac{\partial u'[r;q](x,t)}{\partial\nu}v(x,t)dtds(x) \end{aligned}$$

$$= \int_{\Gamma_1}\int_0^T \left( \frac{rq}{\sqrt{r^2+r'^2}}\frac{\partial u}{\partial t} - \frac{\partial}{\partial s}\left( \frac{rq}{\sqrt{r^2+r'^2}}\frac{\partial u}{\partial s}\right)\right) v(x,t)dtds(x)$$
$$= \int_0^{2\pi} r(\theta)q(\theta)\int_0^T \left( v(x(\theta),t)\frac{\partial u(x(\theta),t)}{\partial t} + \frac{\partial u(x(\theta),t)}{\partial s}\frac{\partial v(x(\theta),t)}{\partial s}\right) dt\ d\theta. \tag{3.7}$$

Finally, we can get (3.3) from (3.6) and (3.7). The proof is complete. □

From Theorem 3.1, we can represent the gradient of the cost functional as

$$\text{grad}\,\bar{J}_\alpha^\delta(r) = 2r(\theta)\int_0^T \left( v(x(\theta),t)\frac{\partial u(x(\theta),t)}{\partial t} + \frac{\partial u(x(\theta),t)}{\partial s}\frac{\partial v(x(\theta),t)}{\partial s}\right) dt + 2\alpha(r(\theta) - r''(\theta)). \tag{3.8}$$

To construct an iteration scheme for minimizing $\bar{J}_\alpha^\delta(r)$ based on the steepest descent algorithm, we need grad $\bar{J}_\alpha^\delta(r)$, which has the expression (3.8). However, the determination of the step size $\beta$ at each iteration is of heavy computational cost, which should be generated by solving a nonlinear equation

$$\frac{\partial \bar{J}_\alpha^\delta(r+\beta q)}{\partial \beta} = 0$$

with respect to $\beta > 0$. To weaken the amount of computations, similarly to the techniques applied in [29], we take the approximate value of step size $\beta$ along the direction $q$. Based on (3.5), we can linearize $\frac{\partial \bar{J}_\alpha^\delta(r+\beta q)}{\partial \beta}$ for $\beta$ as

$$\frac{\partial \bar{J}_\alpha^\delta(r+\beta q)}{\partial \beta} \approx 2\int_{\Gamma_2}\left(\int_0^T \omega u[r]dt - f^\delta\right)\int_0^T \omega u'dt\ ds(x) + 2\alpha\left(\int_0^{2\pi} r(\theta)q(\theta)d\theta + \int_0^{2\pi} r'(\theta)q'(\theta)d\theta\right) + 2\beta\left(\int_{\Gamma_2}\left(\int_0^T \omega u'dt\right)^2 ds(x) + \alpha\int_0^{2\pi} q^2(\theta)d\theta + \alpha\int_0^{2\pi} q'^2(\theta)d\theta\right).$$

By this approximation, the step size $\beta$ can be determined approximately from

$$\beta = -\frac{\int_{\Gamma_2}\left(\int_0^T \omega u[r]dt - f^\delta\right)\int_0^T \omega u'dt\ ds(x) + \alpha\int_0^{2\pi}(r(\theta)q(\theta) + r'(\theta)q'(\theta))d\theta}{\int_{\Gamma_2}\left(\int_0^T \omega u'dt\right)^2 ds(x) + \alpha\int_0^{2\pi}(q^2(\theta) + q'^2(\theta))d\theta}. \tag{3.9}$$

Now we can state our iteration algorithm as follows.

**Algorithm 1** Steepest Descent Iteration Algorithm (SDIA).

**Input:** initial guess $r^0$, tolerance $\varepsilon$ and maximum iteration number $N_{\max}$;
**Output:** $r^F$

1: **for** $k = 0$ **to** $N_{\max}$ **do**
2: Obtain $u[r^k](\cdot,t)|_{\Gamma_1}$, $u[r^k](\cdot,t)|_{\Gamma_2}$ by solving system (1.3);
3: Obtain $v(\cdot,t)|_{\Gamma_1^k}$ by solving system (3.4);
4: Compute $q = -\text{grad}\,\bar{J}_\alpha^\delta|_{r^k}$ based on adjoint system (3.8);
5: **if** $\|q\| < \varepsilon$ or $k = N_{\max}$ **then**
6: $r^F \leftarrow r^k$ and output $r^F$;
7: **end if**
8: Compute $u'[r^k;q](\cdot,t)|_{\Gamma_2}$ based on system (3.2);
9: Determine step size $\beta$ based on equation (3.9);
10: Update $r^{k+1} \leftarrow r^k + \beta q$ and go to step 2;
11: **end for**

## 4. Numerical experiments

We present some numerical results by our proposed algorithm. First, we generate the synthetic data $\{u(x,t), (x,t) \in \Gamma_2 \times [0,T]\}$ by solving the direct problem for known $\Gamma_1$ using the boundary integral equation method (BIEM) [21]. Then, we generate the nonlocal observation data $f^\delta$ for the noisy data of $f$ on $\Gamma_2$.

In testing our reconstruction algorithm, the solutions of the forward problem (1.3), the sensitivity problem (3.2) as well as the adjoint problem (3.4) are solved numerically by the BIEM [21]. To avoid the so-called inverse crime, the setup

of the discretization scheme for the BIEM solving the inverse problem differs from that used for yielding the synthetic data $f$ (and $f^\delta$).

In our two examples with $a = 1$ and different internal boundary $\Gamma_1$ to be sought, we consider the same known external boundary

$$\Gamma_2 = \{x := (x_1, x_2) = 1.5 \times (\cos\theta, \sin\theta),\ \theta \in [0, 2\pi]\}$$

with the excitation heat source

$$\varphi_2(x, t) = 4t^2 \exp(-4t + 2), \quad t \in (0, T) := (0, 1), x \in \Gamma_2, \tag{4.1}$$

and the weight function

$$\omega(t) = \begin{cases} 0, & t \in [0, 0.25) \bigcup (0.75, 1], \\ 1, & t \in [0.25, 0.75]. \end{cases}$$

Under the above configurations, we consider the interior boundary represented by

$$\Gamma_1 := \left\{x :\ x = r^*(\theta)(\cos\theta, \sin\theta) : \theta \in [0, 2\pi]\right\}$$

with polar radius $r^*(\theta)$ for testing the performances of our reconstructions.

In our numerical implementations, we choose the equidistant mesh by setting $\theta_i = \frac{i\pi}{M}$ for $i = 0, 1, \ldots, 2M$ for discretizing the interval $[0, 2\pi]$, while the time internal $[0, T]$ is divided as $N$ subintervals with grids $t_j = \frac{jT}{N}$ for $j = 0, 1, \ldots, N$. For inversion input, the random noisy data $u^\delta(x(\theta_i), t_j)$ are simulated by

$$u^\delta(x(\theta_i), t_j) := u(x(\theta_i), t_j) + \frac{\delta}{\kappa}\text{random}(i, j), \quad (x(\theta_i), t_j) \in \Gamma_2 \times [0, T],$$

where random$(i, j)$ represent random numbers uniformly distributed in $[-1, 1]$ and the constant

$$\kappa := \sqrt{\sum_{i=1}^{2M}\left(\sum_{j=1}^{N}\frac{\omega(t_j)\text{random}(i, j)T}{N}\right)^2 \frac{\pi|x'(\theta_i)|}{M}}.$$

The introduction of the above artificial constant $\kappa$ is for yielding the noisy data $f^\delta$ with suitable noise level $\delta > 0$. By direct computations, the nonlocal observation data $f^\delta$ on $\Gamma_2$ generated from $u^\delta$ is of the noise level

$$\left\|f^\delta - f\right\|_{L^2(\Gamma_2)} = \left\|\int_0^T \omega(t)(u^\delta(\cdot, t) - u(\cdot, t))dt\right\|_{L^2(\Gamma_2)} = \delta.$$

For our reconstructed solution $r^k(\theta)$ at the $k$-th iteration step, the reconstruction performance is checked quantitatively in terms of the following three errors

$$\text{Err}_\alpha(r^{k+1}, r^k) := \left\|r^{k+1} - r^k\right\|_2 = \sqrt{\frac{\pi}{M}\sum_{i=1}^{2M}(r^{k+1}(\theta_i) - r^k(\theta_i))^2},$$

$$\text{Err}_\alpha(r^k, r^*) := \left\|r^k - r^*\right\|_2 = \sqrt{\frac{\pi}{M}\sum_{i=1}^{2M}(r^k(\theta_i) - r^*(\theta_i))^2},$$

$$M_\omega(r^k, f^\delta) := \left\|\int_0^T \omega(t)u[r^k](\cdot, t)dt - f^\delta(\cdot)\right\|_{L^2(\Gamma_2)},$$

where $r^*(\theta)$ is the exact polar radius of $\Gamma_1$ to be sought. These three values reveal the algorithm performances in terms of the iterative convergence, the error between the iterative solution and the exact one and data-fitting error, respectively. We also consider an optimal stopping step defined by

$$N_{0,\alpha} := \{k :\ \arg\min \text{Err}_\alpha(r^k, r^*),\ k = 1, 2, \ldots, N_{\max}\} \tag{4.2}$$

for the reconstructed $\Gamma_1^{N_{0,\alpha}}$ corresponding to $r^{N_{0,\alpha}}(\theta)$ with given regularizing parameter $\alpha > 0$, where $N_{\max}$ is the specified maximum iteration times. Then we choose the appropriate regularization $\alpha^*$ based on the rule (2.3) and the stopping step $N_{0,\alpha}$. However, as shown in our second example, the smallness of $\text{Err}_\alpha(r^k, r^*)$ is not completely equivalent to the satisfactory reconstruction of $r^*$, i.e., the iteration process stopped at $N_{0,\alpha}$ may not be the optimal for satisfactory reconstruction, some other *a-prior* information such as the curvature of $\Gamma_1$ should be embedded into the regularizing scheme furthermore.

**Table 1**
Reconstruction indices for rounded rectangle shape.

| $\alpha$ | $k = N_{0,\alpha}$ | $\mathrm{Err}_\alpha(r^{N_{0,\alpha}}, r^*)$ | $M_\omega(r^{N_{0,\alpha}}, f^\delta)$ | $M_\omega(r^{N_{0,\alpha}}, f)$ |
|---|---|---|---|---|
| $1 \times 10^{-8}$ | 20 | 0.15724 | 0.03041 | 0.010086 |
| $1 \times 10^{-7}$ | 20 | 0.15725 | 0.03042 | 0.010099 |
| $1 \times 10^{-6}$ | 29 | 0.15728 | 0.03031 | 0.010019 |
| $5 \times 10^{-6}$ | 100 | 0.15753 | 0.03032 | 0.010047 |
| $1 \times 10^{-5}$ | 100 | 0.15940 | 0.03103 | 0.010917 |
| $1 \times 10^{-4}$ | 100 | 0.17956 | 0.03336 | 0.014523 |

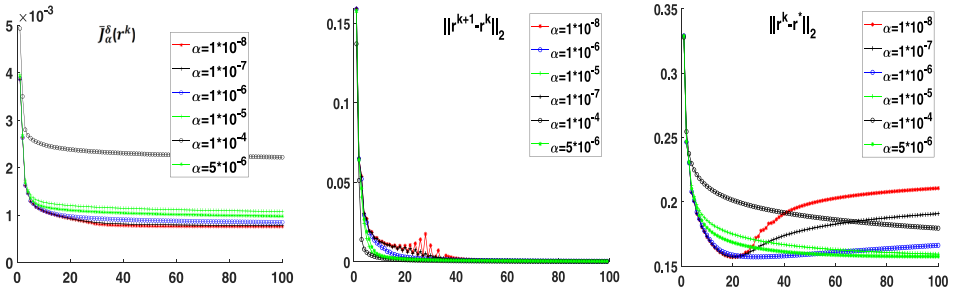


**Fig. 3.** Error distributions with respect to $k$ for rounded rectangle shape.

**Example 1.** Firstly we recover the rounded rectangle $\Gamma_1$ parameterized by its polar radius

$$r^*(\theta) := \left( (\cos\theta)^{10} + \left( \frac{2}{3} \sin\theta \right)^{10} \right)^{-0.1}, \quad \theta \in [0, 2\pi].$$

Obviously, the domain with boundary $\Gamma_1$ is convex and symmetric with respect to the origin.

For the noisy data $u^\delta(x, t)$, we simulate the nonlocal input data $f^\delta$ in $\Gamma_2$ with noise level $\delta = 0.03$. Firstly we analyze the reconstruction behaviors with respect to the regularizing parameter $\alpha$ for the noisy input data. To this end, we set $N_{\max} = 100$ and $\mu = 1.0106$ in (2.3) which yields the regularization parameter $\widehat{\alpha} = 1 \times 10^{-6}$ approximatively. The related three indices are given in Table 1. To compare the reconstruction performances for different regularizing parameters, we also show the indices for the other five values of $\alpha = 1 \times 10^{-8}, 1 \times 10^{-7}, 5 \times 10^{-6}, 1 \times 10^{-5}, 1 \times 10^{-4}$ in Table 1.

From this table, we see that although both $\mathrm{Err}_\alpha(r^{N_{0,\alpha}}, r^*)$ and $M_\omega(r^{N_{0,\alpha}}, f^\delta)$ are not sensitive to $\alpha$, $\widehat{\alpha}$ determined from our strategy is indeed the optimal value for $M_\omega(r^{N_{0,\alpha}}, f^\delta)$ and $M_\omega(r^{N_{0,\alpha}}, f)$. Moreover, we also have for this optimal value $\widehat{\alpha}$ that the data-fitting error

$$M_\omega(r^{N_{0,\widehat{\alpha}}}, f) = 0.010019 < 0.03 = \delta,$$

which means our strategy leads to better date-fit error, as compared with the theoretical error bound $M_\omega(r^{N_{0,\widehat{\alpha}}}, f) \le (\mu + 1)\delta$. This performance supports Theorem 2.5 in Section 2 quantitatively.

To show the iterative performances, three indices, namely, $\bar{J}_\alpha^\delta(r^k)$ and $\mathrm{Err}_\alpha(r^{k+1}, r^k)$ as well as $\mathrm{Err}_\alpha(r^k, r^*)$ with respect to the iteration step $k$ are shown in Fig. 3 for different values of $\alpha$. We find that, although both $\bar{J}_\alpha^\delta(r^k)$ and $\mathrm{Err}_\alpha(r^{k+1}, r^k)$ are decreasing in the iteration process, there exists some optimal step $k$ which minimizes the $L^2$ error $\mathrm{Err}_\alpha(r^k, r^*)$. This is reasonable, since our iterative process only decreases the cost functional $\bar{J}_\alpha^\delta(r^k)$. In addition, the iterative solution $r^{N_{0,\alpha}}$ from our strategy is indeed optimal of $\mathrm{Err}_\alpha(r^k, r^*)$ among all iteration steps $k = 1, \ldots, N_{\max}$, as shown in the third column of Fig. 3.

Of course, the above three quantitative values are only artificial indices for our reconstructions. The actual evaluation criterion on the algorithm should be the reconstruction effect. So we show the reconstruction performances with $\alpha = 1 \times 10^{-8}, 1 \times 10^{-6}, 1 \times 10^{-4}$ in Fig. 4 geometrically, where the known external boundary $\Gamma_2$, exact internal boundary $\Gamma_1$, our initial guess $\Gamma_0$ as well as the reconstructed $\Gamma_1^k$ are also shown simultaneously. Since $N_{0,\alpha} = N_{\max}$ for $\alpha = 1 \times 10^{-4}$, the reconstruction $\Gamma_1^{N_{0,\alpha}}$ is the same as $\Gamma_1^{N_{\max}}$ in the third column of Fig. 4. Moreover, the reconstruction $\Gamma_1^{N_{0,\alpha}}$ in the first row of Fig. 4 is indeed better than $\Gamma_1^{N_{\max}}$ in the second row of Fig. 4 obviously for $\alpha = 1 \times 10^{-8}$ and $\alpha = 1 \times 10^{-6}$, which means that there exists some optimal step $k$ for recovering $\Gamma_1$ approximately, although $\bar{J}_\alpha^\delta(r^k)$ is always decreasing with respect to $k$. On the other hand, the reconstruction $\Gamma_1^{N_{0,\alpha}}$ in the middle sub-figure (first row) of Fig. 4 from our *a-posterior* choice strategy for $\alpha$ is indeed optimal, compared with the other five reconstructed $\Gamma_1^k$ in this figure.

In the next example, we will show that the $L^2$ error $\mathrm{Err}_\alpha(r^{k+1}, r^*)$ is not always an appropriate index for evaluating the recovery effect of $\Gamma_1$.

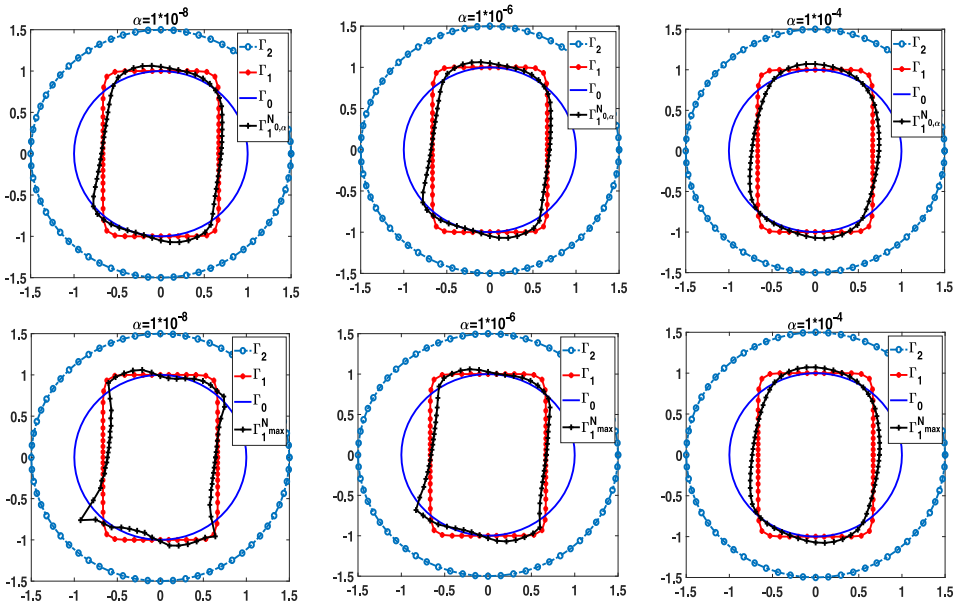


**Fig. 4.** Recovery for optimal and maximum iteration step for rounded rectangle shape.

**Table 2**
Reconstruction indices for kite-shaped $\Gamma_1$ for different $\alpha$.

| $\alpha$ | $k = N_{0,\alpha}$ | $\mathrm{Err}_\alpha(r^{N_{0,\alpha}}, r^*)$ | $M_\omega(r^{N_{0,\alpha}}, f^\delta)$ | $M_\omega(r^{N_{0,\alpha}}, f)$ |
|---|---|---|---|---|
| $1 \times 10^{-9}$ | 2 | 0.50069500 | 0.0257491 | 0.0230288 |
| $1 \times 10^{-8}$ | 2 | 0.50069501 | 0.0257491 | 0.0230288 |
| $1 \times 10^{-7}$ | 2 | 0.50069530 | 0.0257488 | 0.0230285 |
| $5 \times 10^{-7}$ | 2 | 0.50069657 | 0.0257476 | 0.0230271 |
| $1 \times 10^{-6}$ | 2 | 0.50069815 | 0.0257460 | 0.0230254 |
| $1 \times 10^{-5}$ | 2 | 0.50072671 | 0.0257184 | 0.0229950 |

**Example 2.** Consider the kite-shaped internal boundary $\Gamma_1$ parameterized by

$$\Gamma_1 := \{(x_1, x_2) := (0.5\cos\theta + 0.325\cos 2\theta - 0.325, 0.75\sin\theta) : \theta \in [0, 2\pi]\}$$

with the polar radius

$$r^*(\theta) = \sqrt{0.144375 - 0.325\cos\theta + 0.735\sin^2\theta + 0.325\cos\theta\cos 2\theta + 0.325^2\cos^2 2\theta},$$

which is non-convex and asymmetric.

We also test the reconstruction performances with respect to different regularization parameters $\alpha$. For this model, we simulate the boundary input data $f^\delta$ in $\Gamma_2$ with noisy level $\delta = 0.01$. Moreover, we take $N_{\max} = 100$ with initial guess $r^0(\theta) = 1$ in our iteration process, while $\mu = 2.5749$ in (2.3) is specified to yield the regularizing parameter $\widehat{\alpha} = 1 \times 10^{-7}$ approximatively.

We firstly show the reconstruction performances in terms of $\mathrm{Err}_\alpha(r^k, r^*)$, $M_\omega(r^{N_{0,\alpha}}, f^\delta)$ and $M_\omega(r^{N_{0,\alpha}}, f)$ quantitatively for different values of $\alpha$ in Table 2. One important observation is that, if we measure the optimal step in terms of (4.2), then both the optimal step $N_{0,\alpha}$ and the $L^2$ error $\mathrm{Err}_\alpha(r^{N_{0,\alpha}}, r^*)$ are not sensitive to $\alpha > 0$.

We also show the reconstruction performances with respect to the iteration step $k$ for different $\alpha$ in Fig. 5. It can be found that $\bar{J}_\alpha^\delta(r^k)$ is decreasing and $\mathrm{Err}_\alpha(r^{k+1}, r^k)$ is decreasing with small disturbance, which support our reconstruction algorithm quantitatively. However, although there exists some optimal step $N_{0,\alpha}$ which minimizes $\mathrm{Err}_\alpha(r^k, r^*)$, the actual reconstruction behavior may not be optimal at such a step $N_{0,\alpha}$. Such an observation can be found in Fig. 6 for three different values $\alpha = 1 \times 10^{-9}, 1 \times 10^{-7}, 1 \times 10^{-5}$. Obviously, the reconstructions $\Gamma_1^k$ for $k = N_{\max}$ are better than those for $k = N_{0,\alpha}$ in both cases. Noticing that $\Gamma_1$ in this example is non-convex, these numerical observations remind us that, to indicate the reconstruction performances, the $L^2$ error $\mathrm{Err}_\alpha(r^k, r^*)$ for $\Gamma_1$ of general shape is not sufficient, more quantitative indices such as the curvature of the curve should be introduced, which will be the topic in further studies.

On the other hand, from the second row of Fig. 6, we see that $\Gamma_1^{N\max}$ with respect to $\alpha = 1 \times 10^{-7}$ is indeed optimal, compared with the other five reconstructed $\Gamma_1^k$. Due to the above observation, we then take the artificial parameter $\alpha^* = 1 \times 10^{-7}$ and the optimal stop step $k = N_{\max} = 100$ to yield our reconstructions.

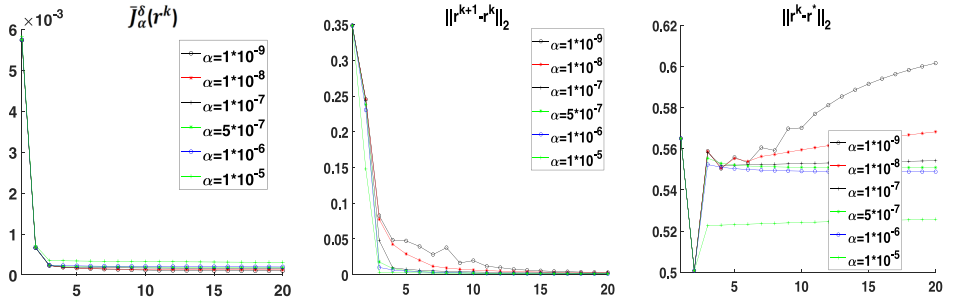


**Fig. 5.** Error distributions with respect to $k$ for different $\alpha$ for kited-shape $\Gamma_1$.

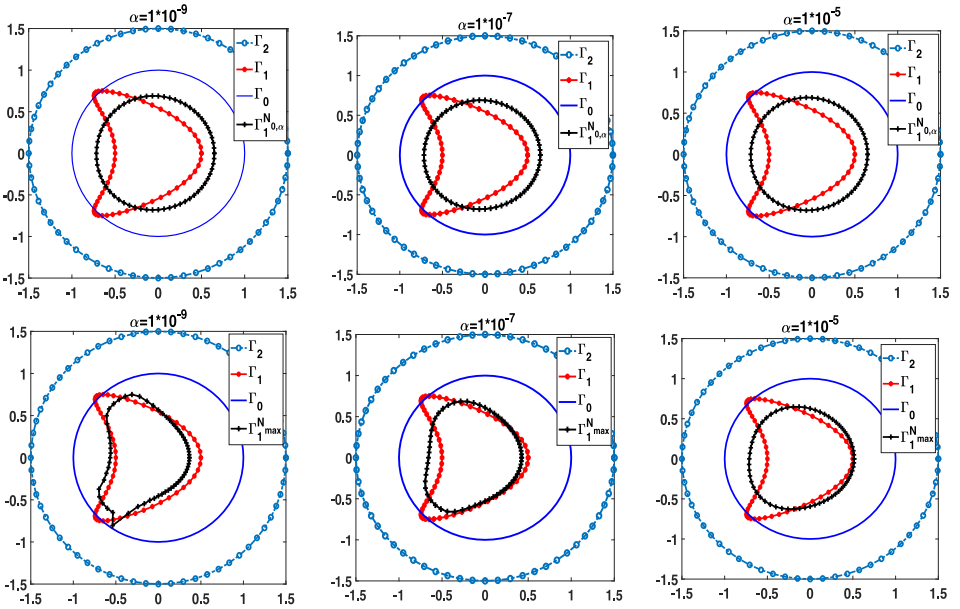


**Fig. 6.** Reconstruction performances of different $k$ for kited-shape boundary.

## 5. Conclusions

We have considered a cavity detection problem in a two-dimensioned heat conductive medium from extra time-average temperature measurement on the outer boundary of the medium. For this inverse problem, under the starlike assumption for the cavity shape, we identify the radius function of the cavity. However, the uniqueness of solution still remains an open issue of future research.

We firstly construct a Tikhonov regularizing functional for recovering the radius function stably, and then we establish the existence of the minimizer of the cost functional. Since the solution of the inverse problem may not be unique, we define the minimum norm solution $r^+$. Moreover, we also prove the uniqueness of the minimum norm solution under certain conditions. The error estimates between the regularizing solution $r^{\alpha,\delta}$ and $r^+$ under the *a-posterior* choice strategy for the regularizing parameter and some source condition are rigorously established. Finally, we propose a steepest descent iteration algorithm for the numerical implementations, based on the adjoint and sensitivity problems of the original problem.

For the numerical examples, the parameter $\mu$ in (2.3) is chosen artificially. The convex and symmetric Example 1 reveals that *a-posterior* choice strategy for $\alpha$ is indeed optimal, and the numerical performance supports Theorem 2.5 quantitatively. However, for the non-convex and asymmetric Example 2, the $L^2$ error $\mathrm{Err}_\alpha(r^k, r^*)$ is not always an appropriate index for evaluating the recovery effect of the unknown cavity. The numerical observations reveal that more quantitative indices such as the curvature of the curve should be introduced to check the reconstruction performance, which will be the topic in further studies.

## Acknowledgments

This work is supported by the Research Start-up Fund of NUIST (Grant/Award No. 2017r094), the Natural Science Foundation of the Jiangsu Higher Education Institutions of China under Grant 19KJB110018 and NSFC (Nos. 11901308, 11601240). The third author is supported by NSFC (Nos. 11971104, 11421110002). This work is also supported by Nanjing Center of Applied Mathematics.

## References

[1] D.H. Chen, D.J. Jiang, J. Zou, Convergence rates of Tikhonov regularizations for elliptic and parabolic inverse radiativity problems, Inverse Problems 36 (7) (2020) 075001.
[2] D.N. Hào, P.X. Thanh, D. Lesnic, Determination of the heat transfer coefficients in transient heat conduction, Inverse Problems 29 (9) (2013) 095020.
[3] D.N. Hào, B.V. Huong, N.T.N. Oanh, P.X. Thanh, Determination of a term in the right-hand side of parabolic equations, J. Comput. Appl. Math. 309 (2017) 28–43.
[4] H.T. Nguyen, V.A. Khoa, V.A. Vo, Analysis of a quasi-reversibility method for a terminal value quasi-linear parabolic problem with measurements, SIAM J. Math. Anal. 51 (1) (2019) 60–85.
[5] R. Julius, T. Fergy, A. Hideyuki, Shape optimization approach to defect-shape identification with convective boundary condition via partial boundary measurement, Japan. J. Ind. Appl. Math. 36 (1) (2019) 131–176.
[6] T. Kurahashi, K. Maruoka, T. Iyama, Numerical shape identification of cavity in three dimensions based on thermal non-destructive testing data, Eng. Optim. 49 (3) (2017) 434–448.
[7] C.I. Castanedo, J. Piau, S. Guilbert, N.P. Avdelidis, M. Genest, A. Bendada, X.P.V. Maldague, Comparative study of active thermography techniques for the nondestructive evaluation of honeycomb structures, Res. Nondestruct. Eval. 20 (2009) 1–31.
[8] A. Kostina, O. Plekhov, S. Aizikovich, Numerical simulation of subsurface defect identification by pulsed thermography and improvement of this technique for noisy data, Frat. Integr. Strut. 50 (2019) 667–683.
[9] A. Friedman, Partial Differential Equations of Parabolic Type, Prentice Hall, Englewood Cliffs, 1964.
[10] J.L. Lions, E. Magenes, Non-Homogeneous Boundary Value Problems and Applications, Vol.2, Springer-Verlag, Berlin, 1972.
[11] O.A. Ladyzhenskaia, V.A. Solonnikov, N.N. Uralceva, Linear and Quasilinear Equations of Parabolic Type, AMS, Providence, 1968.
[12] D.L. Balageas, A.A. Deom, D.M. Boscher, Characterization and nondestructive testing of carbon-epoxy composites by a pulsed photothermal method, Mater. Eval. 45 (4) (1987) 461–465.
[13] J.J. Liu, Y.C. Wang, On the reconstruction of boundary impedance of heat conduction system from nonlocal measurement, Inverse Problems 32 (7) (2016) 075002.
[14] L. Jean, A Course on Damage Mechanics, Springer-Verlag, Berlin, 1996.
[15] A. Henrot, J. Sokolowski, A shape optimization problem for the heat equation, Opt. Control: Theory Algorithms Appl. 15 (1998) 204–223.
[16] G. Nakamura, H.B. Wang, Numerical reconstruction of unknown robin inclusions inside a heat conductor by a non-iterative method, Inverse Problems 33 (5) (2017) 055002.
[17] H.B. Wang, Y. Li, Numerical solution of an inverse boundary value problem for the heat equation with unknown inclusions, J. Comput. Phys. 369 (2018) 1–15.
[18] H. Harbrecht, J. Tausch, On the numerical solution of a shape optimization problem for the heat equation, SIAM J. Sci. Comput. 35 (1) (2013) A104–A121.
[19] H.T. Banks, F. Kojima, W.P. Winfree, Boundary estimation problems arising in thermal tomography, Inverse Problems 6 (6) (1990) 897–921.
[20] J. Sokolowski, Shape sensitivity analysis of boundary optimal control problems for parabolic systems, SIAM J. Control Opt. 26 (4) (1988) 763–787.
[21] R. Chapko, R. Kress, J.R. Yoon, An inverse boundary value problem for the heat equation: the Neumann condition, Inverse Problems 15 (4) (1999) 1033–1046.
[22] R. Chapko, P. Kugler, A comparison of the Landweber method and the Gauss–Newton method for an inverse parabolic boundary value problem, J. Comput. Appl. Math. 169 (1) (2004) 183–196.
[23] C.D. Pagani, D. Pierotti, Identifiability problems of defects with the Robin condition, Inverse Problems 25 (12) (2009) 055007.
[24] F. Caubet, M. Dambrine, D. Kateb, Shape optimization methods for the inverse obstacle problem with generalized impedance boundary conditions, Inverse Problems 29 (11) (2013) 115011.
[25] G. Inglese, An inverse problem in corrosion detection, Inverse Problems 13 (4) (1997) 977–994.
[26] R. Mendoza, S. Keeling, A two-phase segmentation approach to the impedance tomography problem, Inverse Problems 33 (1) (2017) 015001.
[27] S.W. Anzengruber, R. Ramlau, Convergence rates for Morozov's discrepancy principle using variational inequalities, Inverse Problems 27 (10) (2011) 105007.
[28] Y.C. Wang, J.J. Liu, On the edge detection of an image by numerical differentiations for gray function, Math. Methods Appl. Sci. 41 (6) (2018) 2466–2479.
[29] B. Jin, X. Lu, Numerical identification of a robin coefficient in parabolic problems, Math. Comp. 81 (279) (2012) 1369–1398.